# Comparing numerical and experimental approaches for the stochastic modeling of the bouncing of a boulder on a coarse soil

Franck Bourrier, François Nicot, Nicolas Eckert, Félix Darve

# Comparing numerical and experimental approaches for the stochastic modeling of the bouncing of a boulder on a coarse soil

**Franck Bourrier* — François Nicot* — Nicolas Eckert***
**Félix Darve****

** Cemagref, UR ETNA*
*2, rue de la Papeterie, BP 76, F-38402 Saint-Martin-d'Hères Cedex, France*
*{franck.bourrier, françois.nicot, nicolas.eckert}@cemagref.fr*

*** Laboratoire 3S-R, INPG, UJF, CNRS*
*Domaine Universitaire, BP 53, F-38041 Grenoble Cedex 9, France*
*felix.darve@inpg.fr*

ABSTRACT. *This paper proposes numerical investigations for the stochastic modeling of a boulder impacting a coarse granular soil. The soil is considered as a noncohesive granular medium using a discrete element method and the soil model is calibrated compared to results from half-scale experiments. Based on this numerical model, an extensive numerical simulation campaign is carried out. The statistical analysis of the numerical results allows the definition of a stochastic bouncing model that quantifies most of the variability of the numerical results. Comparisons with classical bouncing models in the field of trajectory analysis highlight that this model expands classical approaches. The comparison of results from real-scale experiments to trajectory simulations based on the stochastic model show the relevance of the proposed approach to modeling rockfall trajectories.*

RÉSUMÉ. *Une modélisation stochastique de l'impact d'un bloc sur un sol grossier basée sur un modèle aux éléments discrets est proposée. Le sol est considéré comme un milieu granulaire non cohésif et le modèle d'impact est calibré par comparaison à des résultats d'essais à échelle réduite. Une campagne de simulation extensive est menée à l'aide de ce modèle. L'analyse statistique des résultats de simulation permet de définir une loi stochastique de rebond capable de quantifier une grande partie de la variabilité de ces résultats. La comparaison aux modèles de rebond classiques en analyse trajectographique montre que le modèle proposé est une extension des approches classiques. La comparaison entre les résultats d'essais de terrain et les simulations de ces essais à l'aide du modèle stochastique met en évidence la pertinence de l'approche proposée pour modéliser les trajectoires des blocs.*

KEYWORDS: *rockfall hazard, impact, discrete element method, stochastic, trajectory analysis.*

MOTS-CLÉS : *risque de chute de blocs, méthode des éléments discrets, stochastique, analyse trajectographique.*

## 1. Introduction

Natural hazard assessment is a major challenge in mountainous zones. Rockfall is a very common and dangerous phenomenon, even if the boulders involved are relatively small. Rockfall is a small mass movement that consists in the removal of a superficial boulder from a cliff face or a talus slope. Endangered residential areas and infrastructures must be protected against the risk associated with rockfall events. Locating and designing defense structures against rockfall such as restraining nets or barrier fences is a difficult task in which the prediction of the trajectories of the potentially falling boulders is one of the key points. Trajectory analyses are therefore performed to inform practitioners on the potential trajectories of the falling boulder within the area to be protected.

In the context of trajectory analysis, the information available on the local configuration of the soil near the impact point and on the incident kinematic parameters of the boulder is not sufficient for a relevant deterministic prediction of boulder bouncing. The high variability of these parameters (Laouafa *et al.*, 2003) makes exhaustive deterministic modeling of the impact of the boulder on the soil impossible. To overcome these difficulties, stochastic approaches have been proposed for modeling the impact (Paronuzzi, 1989; Pfeiffer and Bowen, 1989; Azzoni *et al.*, 1995; Guzzetti *et al.*, 2002; Agliardi and Crosta, 2003). However, such approaches only provide a simplified empirical simulation of the variability associated with the impact phenomenon.

The aim of the present paper is to define a stochastic bouncing model that can properly model the variability of the impact phenomenon in the case of the interaction of a boulder with a scree slope. Because of the complexity of the phenomenon (Bourrier *et al.*, 2008), large data sets analyzed using advanced statistical methods are necessary to define a reliable stochastic model (Bourrier *et al.*, 2007). Results from rockfall events or field experiments are not directly usable because either the data set is incomplete (rockfall events) or reproducible impact conditions are difficult to obtain (field experiments). On the other hand, simulations are well adapted because various geometrical configurations (grading curve, particle arrangement) can be considered, and, for each geometrical configuration studied, a large set of incident conditions can be explored.

Therefore, in this approach we chose to use numerical simulations to define the stochastic bouncing model. The first step of the procedure is numerically modeling, in a 2D context, a single interaction between the falling boulder and the scree using the discrete element method (DEM). The validity of the DEM simulation procedure is evaluated and calibrated by comparing results from half-scale experiments with simulations using the DEM model under the same conditions.

In the second step, an extensive simulation campaign was carried out, made up of impact simulations for varying incident kinematic conditions of the boulder and varying local configurations of the soil. The numerical results are analyzed using

advanced statistical modeling. The stochastic bouncing model obtained is then exhaustively presented and a sensitivity analysis is done to determine the validity domain of the model proposed.

Finally, the stochastic bouncing model is compared with data from real-scale experiments. To do so, the 2D stochastic bouncing model is integrated into a 3D trajectory analysis software. On the basis of the results obtained, the relevance of the stochastic bouncing model is discussed.

## 2. Numerical simulation of impacts using the DEM

### 2.1. *DEM impact model*

The scree slope is an assembly composed of several rocks of various sizes and shapes. During the impact, a dynamical loading attributable to the interaction with the boulder is applied to the scree slope. Assuming that rocks composing the talus slope can be considered rigid locally deformable 2D bodies, the Particle Flow Code 2D software (Itasca, 1999) based on the DEM (Cundall and Strack, 1979) is used. In the DEM, particles are subjected to body forces, limited to gravitational forces in our case, as well as to contact forces. Contact forces are applied to neighboring particles in contact. For a given time step, once body and contact forces have been computed, the translational and rotational velocities of the particles are determined by solving the balance equation. The resulting displacements of the particles are used to update particle locations for the next time step.

The normal and tangent contact forces acting between two particles are calculated using a hypoelastic contact law (Cundall, 1988) based on an approximation of the Hertz–Mindlin theory (Mindlin and Deresiewicz, 1953). The contact law formulation relates both the normal and tangential incremental contact forces $dF_n$ and $dF_t$ to the normal and the tangential incremental interpenetrations $du_n$ and $du_t$ using the relations:

$$dF_n = \frac{3}{2} K_n \sqrt{u_n}\, du_n \qquad [1]$$

$$dF_t = K_t du_t \xi (F_n \tan\varphi - F_t) \qquad [2]$$

with:

$$K_n = \frac{2\sqrt{2R_p}\,G}{3(1-\nu)} \qquad [3]$$

$$K_t = 2\frac{(3G^2(1-\nu)R_p)^{1/3}}{2-\nu}F_n^{1/3} \quad [4]$$

and

$$R_p = \frac{2R_1R_2}{R_1+R_2} \quad [5]$$

where $\varphi$ is the local friction angle and $K_n$ and $K_t$ are normal and tangential stiffness coefficients depending on the radii $R_1$ and $R_2$ of the particles involved, shear modulus $G$, and Poisson ratio $\nu$. $\xi$ is the Heaviside function: $\xi(x) = 1$ if $x > 0$ and $\xi(x) = 0$ if $x \leq 0$.

The Hertz–Mindlin model takes frictional processes between adjoining particles into account. Other dissipation sources also exist within real granular soils subjected to dynamical loadings, such as local yielding near the contact surface, crack propagation, and rock breakage. However, in the context of the simulations where a boulder is approximately the same size as the soil particles, local plastic dissipation within the particle body is assumed to be negligible compared to frictional dissipation in a first approximation (Oger *et al*., 2005).

Contact forces are governed by three parameters set at classical values for rocks (Goodman, 1980): the shear modulus $G$ is set at 40 *GPa*, the value of the Poisson ratio $\nu$ is set at 0.25 and the local friction angle $\varphi$ is 30°. In addition, the density $\rho$ of the boulder and of the soil particles is set at 2650 $kg/m^3$.

Given that natural scree are polydisperse granular assemblies (Kirkby and Statham, 1975), the ratio between the mass of the smaller rock and of the larger rock of the soil is set at 10. This also prevents the calculation time step from decreasing. The mean equivalent radius of the soil particles is set at $R_m$ = 0.3 *m*. To limit the number of varying parameters, simulations are performed for an impact of a spherical boulder on the soil. The diameter of the boulder $R_b$ can vary from 0.5 $R_m$ to 5 $R_m$. This context highlights the role of the local geometrical configuration in the variability of the impact phenomenon (Bourrier et al., 2008). The influence of soil particle shape is also explored by defining different soil samples composed of either spherical particles or clump particles. Clumps are indivisible assemblies of spherical particles used to model the shape of soil rocks in a more realistic way (Bertrand *et al*., 2006; Nicot *et al*., 2007; Deluzarche and Cambou, 2006). Clump shape is nearly rectangular and is governed by the ratio of particle length to width, which is randomly chosen between 1 and 4 to account for shape variability within a talus slope (Figure 1).

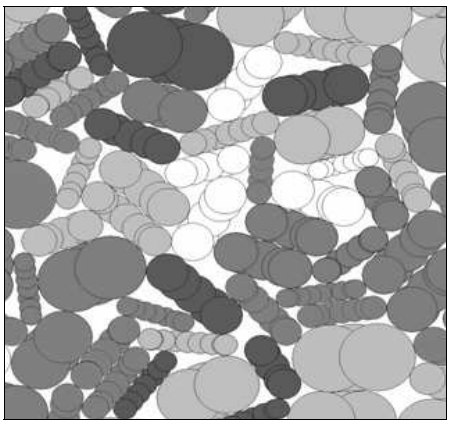

**Figure 1.** *Clump particle assembly*

The soil sample is generated from distinct particles subjected to gravitational forces only. Particles are therefore first randomly generated inside an empty sample limited by rigid walls. The initial particle locations are determined to prevent initial interactions. Gravitational forces are applied to all particles and a calculation procedure is run until the total kinetic energy of the system lowers a set value (Figure 2). The porosity of the generated sample can be precisely controlled by calibrating the value of the local friction angle during the generation of the sample. After sample generation, the local friction angle is set at $\varphi = 30°$ whatever the value of this parameter used during sample generation. At the end of the generation procedure, sample depth $H$ is set at $12.5\,R_m$. The values used for the main geometrical and mechanical parameters of the soil sample are summarized in Table 1.

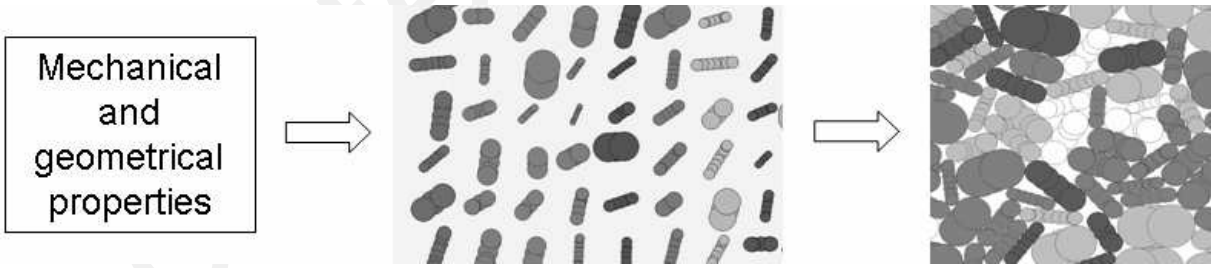


**Figure 2.** *Sample generation*

The impacting boulder is a sphere. Using such a simple shape does not allow exploring the non negligible influence of the boulder shape on the bouncing (Guzzetti *et al*., 2002). However, in a first approximation, the choice was made to use impacting spheres for two reasons. First, most of classical rockfall trajectory simulation codes use spheres (Guzzetti *et al*., 2002). Second, if complex impacting boulder shape had been used, the characterization of the boulder shape would have been a difficult task due to the important variability of boulder shapes in practice.

Once the sample has been generated, each impact simulation first consists in defining the impact point. The boulder radius is then set along with the incident kinematics conditions. Incident kinematic conditions are fully defined by the magnitude of the incident velocity $V^{in}$, the incident angle $\alpha^{in}$, and the incident rotational velocity $\omega^{in}$ (Figure 3). These parameters are directly related to the normal and tangential velocity components by the relations:

$$v_x^{in} = V^{in} \sin(\alpha^{in}) \quad [6]$$

$$v_y^{in} = -V^{in} \cos(\alpha^{in}) \quad [7]$$

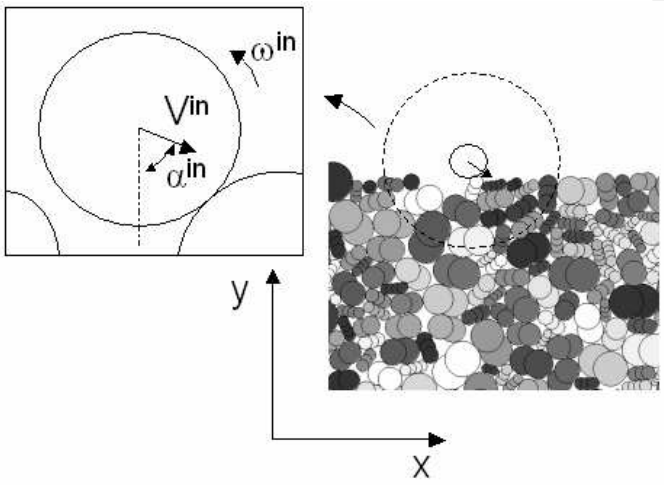


**Figure 3.** *Incident kinematical conditions*

**Table 1.** *Geometrical and mechanical parameters used in the simulations*

| Parameter | Varying domain |
|---|---|
| Shear modulus $G$ | $G = 40\ GPa$ |
| Poisson ratio $v$ | $v = 0.25$ |
| Local friction angle $\varphi$ | $\varphi = 30°$ |
| Rocks density $\rho$ | $\rho = 2650\ kg/m^3$ |
| Ratio of the smaller ($m_{min}$) to the larger ($m_{max}$) rock mass | $m_{max}/\ m_{min} = 10$ |
| Mean equivalent radius of soil rocks $R_m$ | $R_m = 0.3\ m$ |
| Ratio of soil rocks length $L$ to width $w$ | $1 \leq L/w \leq 4$ |
| Impacting boulder radius $R_b$ | $0.5R_m \leq R_b \leq 5R_m$ |
| Sample depth $H$ | $H = 12.5R_m$ |

A minimum distance $d_i$ between two impact points is also set to limit an unnecessary refinement of the results. Preliminary numerical investigations have

shown that a minimum of $N$ = 100 impact points distant from $d_i$ = 0.05 *m* has to be chosen to ensure stable mean values and standard deviations of the components of the reflected velocity (Bourrier *et al*., 2007). It is worth noting that all impact points are located far enough from the lateral walls of the sample to avoid disturbances from the lateral walls (Bourrier *et al*., 2007). For each impact simulation, reflected velocities are collected when the normal component of the boulder velocity reaches its maximum value, which usually occurs after the last contact between the boulder and the soil particles.

## 2.2. *Half-scale experiments*

The validity of the DEM impact model is evaluated by comparing predictions using this model with results from half-scale experiments.

The half-scale experiments consist of the impact of a rock, whose equivalent diameter is 6.8 *cm*, on a coarse soil composed of limestone rocks having approximately the same size as the impacting rock. The impacting rock is a quasi-spherical granite projectile that limits projectile breakage during impact and facilitates the calculation of the velocity of the impacting rock. A specific projectile dropping device was designed and calibrated in order to control the magnitude and the direction of the incident velocity of the projectile. The incident velocity of the projectile is 6 *m/s*, the incidence angle $\alpha^{in}$ (Figure 4) can reach values from 0° to 75°and the incident rotational velocity is always nil. The incident velocity belongs to the *xy* plane, called incident plane (Figure 4). The component of the incident velocity along the *z* axis is therefore always nil.

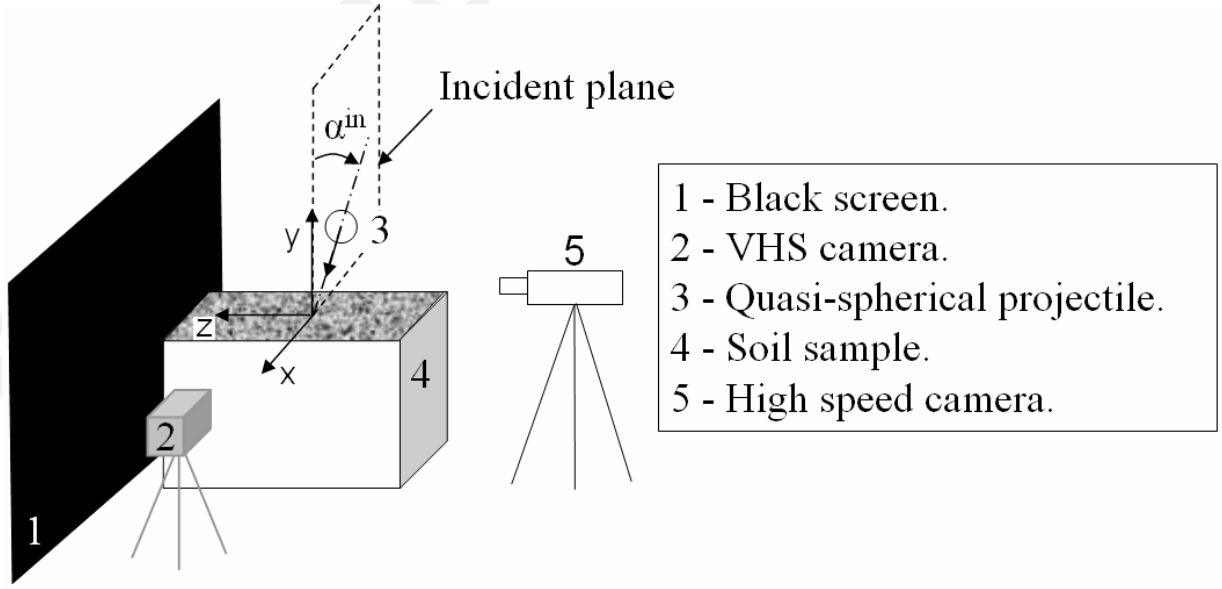


**Figure 4.** *Experimental set-up*

The impact experiments were filmed in the *xy* plane using a high-speed camera and in the *yz* plane using a VHS camera (Figure 4). The analysis of VHS films showed that the reflected velocity of the boulder along the *z* axis was negligible toward the other components of the reflected velocity. Image processing of the films from the high-speed camera therefore allowed the calculation of the normal and tangential components of the reflected velocity of the boulder. More than 100 impact experiments were conducted for varying incidence angles. The values of the incidence angle varied from 0° to 75° and the same number of impact experiments were conducted for each incidence angle value explored (0°, 15°, 30°, 45°, 60°, 75°).

### 2.3. *DEM impact model validation*

In order to remove the effects of scale changes while evaluating the relevance of the DEM model compared to the experimental results, the DEM model described in Sub-Section 2.1 was adapted. The characteristics of the numerical model of the impact were therefore defined to match the measured properties of the experimental soil sample and the experimental incident conditions. The impacting sphere radius was set to the same value as the equivalent radius of the granite rock used in the experiments. Additionally, the numerical incident conditions were similar to the experimental ones and the size of the numerical soil sample was the same as the experimental soil sample. The size of the particles of the numerical soil sample were determined in order to come close to the experimental grading curve and the distribution of the length to width ratio, defined as the ratio of the particles' length to the particles' width, of the rocks composing the experimental soil sample (Figure 5). One can also note that the Hertz–Mindlin contact law is still used and that the values of the mechanical properties of the particles are similar to those defined in Sub-Section 2.1 ($G = 40\ GPa$, $\nu = 0.25$, $\varphi = 30°$, and $\rho = 2650\ kg/m^3$).

The porosity of the numerical soil sample is considered a calibration parameter because no simple relation exists between the 3D porosity of the experimental soil sample and the 2D porosity of the numerical soil sample. The numerical simulations were therefore performed using several numerical soil samples with different 2D porosities.

The simulation results obtained were compared with the experimental results. Both the cumulative distribution functions of the tangential $V_x^{re}$ and normal $V_y^{re}$ to soil surface components of the reflected velocity were compared.

The results highlight a fair accordance between the cumulative distribution functions of the reflected velocity components in the simulations and the experiments (Figure 6). The tangential component $V_x^{re}$ of the velocity was predicted particularly well using the DEM model because, whatever the porosity of the numerical soil sample, the cumulative distribution function of the simulation results was contained within the confidence interval associated with the experimental results (Figure 6). In addition, the porosity of the numerical soil sample did not change the

results for the tangential component $V_x^{re}$. On the contrary, the values of the normal component $V_y^{re}$ strongly depended on the porosity of the numerical soil sample (Figure 6). The dependency of the normal component $V_y^{re}$ on the porosity can be explained by the fact that larger energy dissipation occurs for loose soils than for dense soils due to increases in particles rearrangement and frictional dissipation. The effects of the porosity changes are significant only for the normal component of the velocity because previous simulations (Bourrier *et al.*, 2008) have shown that the energy transfers between the soil and the impacting boulder were mainly associated with the normal component of the velocity.

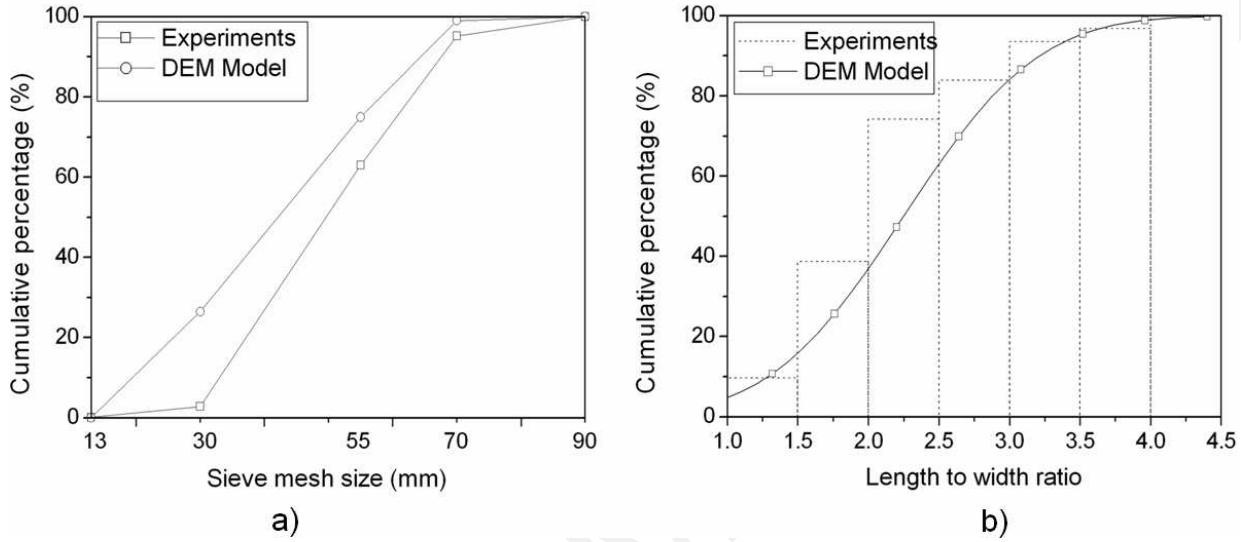


**Figure 5.** *Grading curves (graph a) and length to width ratio distribution (graph b) of the experimental and numerical soil samples*

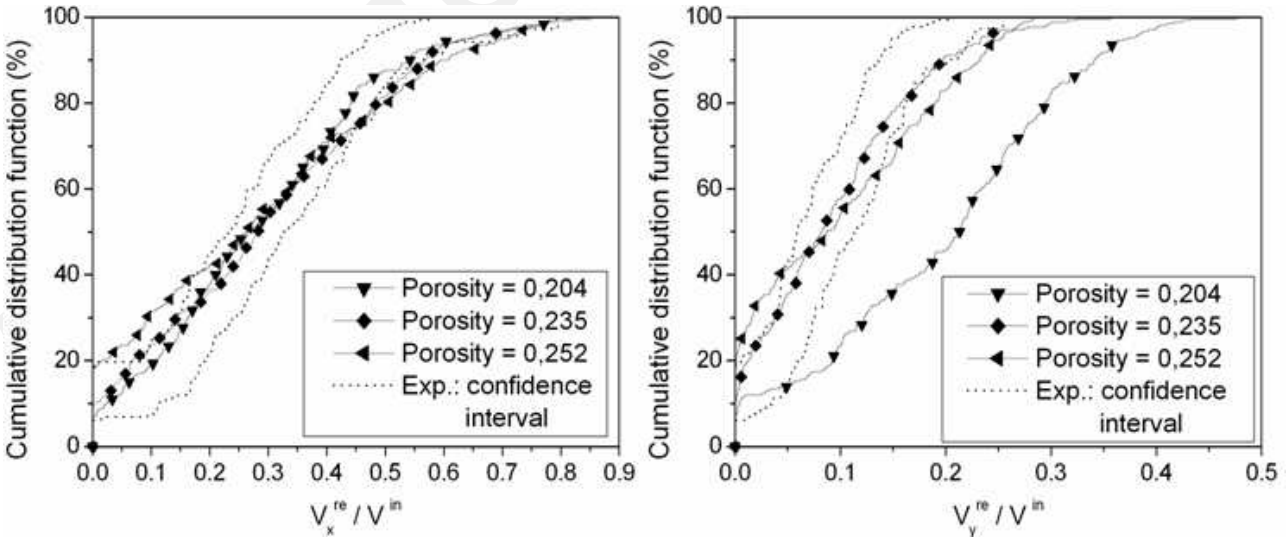


**Figure 6.** *Comparison between the cumulative distribution functions of the tangential $V_x^{re}$ and normal $V_y^{re}$ to soil surface components of the reflected velocity obtained in the experiments and in the simulations. Several simulation results corresponding to impacts on different soil samples of varying porosity are compared with the experimental results*

Despite the dependency of the normal component $V_y^{re}$ on the porosity, one can find a value of the porosity of the numerical soil sample that allows a satisfactory approach to the experimental results for both components $V_x^{re}$ and $V_y^{re}$. This proves that the DEM properly models the impact of a rock on a coarse soil for a reduced number of calibration parameters: the porosity of the soil sample is the only simulation parameter to be calibrated.

## 3. Statistical analysis of the bouncing phenomenon

### 3.1. *Constitution of a database*

As the relevance of the DEM model has been proved, several impact simulations using this model were conducted to explore the variability of the reflected velocity for varying impact points and incident kinematic parameters and for fixed soil and boulder characteristics. The properties of the numerical soil sample correspond to those presented in Sub-Section 2.1. The variability of the reflected velocity was studied for different shapes of soil particles (spheres or clumps) and impacting boulder radii (between 0.5 $R_m$ and 5 $R_m$).

For given properties of the boulder and the soil, several impact simulations were conducted for varying impact points and incident kinematic parameters. First, 100 impact points are precisely defined so that the same impact point can be used for several incident kinematic conditions. For a given impact point, a set of equally distributed incident kinematic parameters was explored. Kinematic parameter values ranged within the limits defined from rockfall events (Azzoni *et al.*, 1991). For each impact point, all the combinations of chosen values for incident kinematic parameters (Table 2) were explored. Collection of the components of the reflected velocity of the boulder for all simulations made it possible to construct a database of numerical results for varying impact points and incident kinematics conditions and for fixed soil properties and boulder size.

**Table 2.** *Values of the incident kinematic parameters*

| Incident parameters | Values explored |
|---|---|
| $V^{in}$ $(m/s)$ | 5, 10, 15, 20, 25 |
| $\alpha^{in}$ $(deg)$ | 0, 15, 30, 45, 60, 75 |
| $\omega^{in}$ $(rad/s)$ | –6, –3, 0, 3, 6 |

### 3.2. *Formulation of the stochastic bouncing model*

To perform the statistical analysis of the simulation results database for given properties of the boulder and the soil, the reflected kinematic parameters of the boulder were computed from the incident kinematic parameters of the boulder by means of an operator $\tilde{f}$. A generalized velocity vector **V** composed of a normal velocity component $v_y$, a tangential velocity component $v_x$, and a rotational velocity $\omega$ (Figure 3) can properly describe the kinematic parameters of the boulder such as:

$$\mathbf{V} = \begin{pmatrix} v_x & v_y & R_b\omega \end{pmatrix}^t \quad [8]$$

Incident $\mathbf{V^{in}}$ and reflected $\mathbf{V^{re}}$ generalized velocity vectors of the rock are related as follows:

$$\mathbf{V^{re}} = \tilde{f}(\mathbf{V^{in}}) \quad [9]$$

Assuming that there is a Taylor series expansion of the operator $\tilde{f}$ with respect to all components of the incident velocity vector $\mathbf{V^{in}}$, the first-order truncation of the Taylor series expansion of $\tilde{f}$ defined in Eq. 8 gives the definition of the operator **A**. The operator **A** associates the reflected velocity vector $\mathbf{V^{re}}$ with the incident vector $\mathbf{V^{in}}$:

$$\mathbf{V^{re}} = \mathbf{A}\mathbf{V^{in}} + \mathbf{R}(\mathbf{V^{in}}) \quad [10]$$

with,

$$\mathbf{A} = \begin{bmatrix} a_{xx} & a_{xy} & a_{x\omega} \\ a_{yx} & a_{yy} & a_{y\omega} \\ a_{\omega x} & a_{\omega y} & a_{\omega\omega} \end{bmatrix},$$

where the parameters $a_i$ are the coefficients of the first-order Taylor series expansion of the operator $\tilde{f}$ and $\mathbf{R(V^{in})}$ is a remainder term denoting the difference between the operator $\tilde{f}$ and its first-order Taylor series expansion.

The high variability of the local soil properties near the impact point and of the incident kinematic conditions induces the operator **A** and the remainder term $\mathbf{R(V^{in})}$ to take very different values. A stochastic bouncing model was therefore developed to account for the variability associated with the operator **A** and the remainder term $\mathbf{R(V^{in})}$ separately. The variability related to the spatial distribution of the soil

particles near the impact point also has to be distinguished from the variability related to the incident kinematic conditions in the stochastic bouncing model.

In order to associate the variability of the operator **A** with the variations in the local geometrical layout of the soil particles near the impact point, the operator **A** was assumed to take a constant value **A** for a given impact point $p$ whatever the set $k$ of incident kinematic parameters. Due to similarities in the macroscopic properties of the soil (porosity, the particles' mechanical properties, grading curve, etc.) for all impact points, it is assumed that the results observed at the different impact points are, in some ways, similar. For a given impact point, the value of the operator **A** is constant for any incident kinematical conditions. In addition, the values of the operator **A** are different from one impact point to the other but, as the impacted soil macroscopic properties are similar for all impact points, all values of **A** are extracted from the same probability distribution function. For varying impact points $p$, the coefficients of the operator **A** were therefore assumed to be sampled from the same normal probability distribution function characterized by a mean vector $\mathbf{M}^{\mathbf{a}}$ and a covariance matrix $\mathbf{\Sigma}^{\mathbf{a}}$.

To quantify the variability associated with **A** and $\mathbf{R(V^{in})}$ separately, the assumption was also made that, whatever the impact point $p$ and the incident kinematic conditions $k$, the reflected velocity vector $\mathbf{V}^{\mathbf{re}}_{pk}$ was sampled from a normal distribution fully defined by a mean vector $\mathbf{A}_p\mathbf{V}^{\mathbf{in}}_{pk}$ and a covariance matrix $\mathbf{\Sigma}$. The covariance matrix $\mathbf{\Sigma}$, which accounts for the proportion of variability of the remainder term $\mathbf{R(V^{in})}$, is constant for all impact points and incident kinematic parameters.

The unknown parameters of the stochastic model are $\mathbf{M}^{\mathbf{a}}$, $\mathbf{\Sigma}^{\mathbf{a}}$, $\mathbf{\Sigma}$. The values of these parameters were obtained by the statistical analysis of the numerical results database using Bayesian inference (Bayes, 1763) and the associated so-called MCMC simulation algorithms (Brooks, 1998; Gilks *et al.*, 2001).

The level of agreement between the model and the data was evaluated by estimating the contribution of the random variable $\mathbf{AV^{in}}$ to the total variability of the results. For this purpose, the percentage ($R$ coefficient) of the total variability of the results that is explained by the random variable $\mathbf{AV^{in}}$ for a given impact point $p$ and for the $i^{th}$ incident component of the reflected velocity vector $\mathbf{V^{re}}$ was assessed. If $R$ = 100%, all the variability of the results is explained by the random variable $\mathbf{AV^{in}}$. This quantity is similar to the $R^2$ statistic classically used while performing a linear regression.

### 3.3. *A simplified formulation of the stochastic bouncing model*

The analysis of the stochastic bouncing model is described for the case of the impact of a spherical boulder having a radius set at $R_b = R_m$ on a soil sample composed of spherical particles. The porosity of the impacted soil sample is 0.204

and the other properties of the soil sample are similar to those defined in Sub-Section 2.1.

The results first show that most of the variability of the reflected velocity is captured by the random variable $\mathbf{AV^{in}}$ because the $R$ coefficient was greater than 85%. The reflected quantities can therefore be correctly predicted using only the random variable $\mathbf{AV^{in}}$ and by omitting the covariance matrix $\mathbf{\Sigma}$. Thus, an admissible simplified formulation of the stochastic bouncing model is:

$$\begin{bmatrix} v_x^{re} \\ v_y^{re} \\ R_b\omega^{re} \end{bmatrix} = \begin{bmatrix} a_{xx} & a_{xy} & a_{x\omega} \\ a_{yx} & a_{yy} & a_{y\omega} \\ a_{\omega x} & a_{\omega y} & a_{\omega\omega} \end{bmatrix} \begin{bmatrix} v_x^{in} \\ v_y^{in} \\ R_b\omega^{in} \end{bmatrix} \quad [11]$$

Correctly predicting the reflected velocity vector using the stochastic bouncing model therefore only requires defining all the coefficients of $\mathbf{M^a}$ and $\mathbf{\Sigma^a}$.

The distribution of each parameter $a_i$ (Figure 7) is a normal distribution that is fully defined by a mean value $m_i^a$, corresponding to the $i^{th}$ component of the mean vector $\mathbf{M^a}$, and a standard deviation $s_i^a$, corresponding to the square root of the $i^{th}$ diagonal term of the covariance matrix ($s_i^a = \sqrt{\mathbf{\Sigma}^a(i,i)}$). This aspect will be considered in Sub-Section 3.4 in order to characterize the sensitivity of the parameters $a_i$ with respect to various mechanical and geometrical characteristics.

The stochastic bouncing model can be compared with classical approaches in the field of trajectory analysis. Classical bouncing models are based on deterministic mechanical analyses. Some models differentiate two interaction types between the boulder and the soil: the falling rock can either roll or bounce onto the soil (Bozzolo and Pamini, 1986; Evans and Hungr, 1993; Kobayashi *et al*., 1990; Azzoni *et al*., 1995), whereas most approaches consider boulder rolling a succession of small bounces. Additionally, very complex bouncing models (Falcetta, 1985; Koo and Chern, 1998; Dimnet and Fremond, 2000) have been developed to model boulder bouncing, which allows thorough description of the plastic, frictional, or viscous dynamical behavior of the soil during impact. Although the differences between the previously described approaches should not be omitted, the bounce is most often simulated using one or two coefficients. The most commonly used coefficients (Guzzetti *et al*., 2002) are the tangential $R_t$ and the normal $R_n$ restitution coefficients:

$$\begin{bmatrix} v_x^{re} \\ v_y^{re} \end{bmatrix} = \begin{bmatrix} R_t & 0 \\ 0 & R_n \end{bmatrix} \begin{bmatrix} v_x^{in} \\ v_y^{in} \end{bmatrix} \quad [12]$$

The variability of the bouncing phenomenon is, in most cases, introduced at a later time by modeling the restitution coefficients as independent random variables

that follow user-defined distributions (Agliardi and Crosta, 2003; Frattini *et al*., 2008; Jaboyedoff *et al*., 2005).

The use of classical restitution coefficients $R_t$ and $R_n$ induces that each component of the reflected velocity only depends on one of the components of the incident velocity vector (Equation [12]). The classical models based on restitution coefficients therefore only account for the diagonal terms of the operator **A** ($a_{xx}$ and $a_{yy,}$ in particular). On the contrary, in the stochastic bouncing model, all the terms of the operator **A** are used. As a result, all the components of the reflected velocity vector depend heavily on all the incident kinematic parameters (Equation [11]). Moreover, contrary to classical approaches, the model proposed is directly developed in a global stochastic framework. The stochastic bouncing model proposed therefore constitutes an extension to classical models that reflects the coupling between the incident kinematic parameters and allows proper description of the variability of the reflected velocity.

### 3.4. *Influence of soil particle shape and boulder size*

The influence of the mechanical and geometrical characteristics of the soil and the boulder is investigated. The values of the model's parameters can vary depending on the soil and boulder characteristics. Since an exhaustive parametrical study would be very long, we chose to limit the investigations to the influence of the parameters that are commonly considered by practitioners (Dorren *et al*., 2006). We therefore limited our investigations to the analysis of the influence of the size and the shape of the soil particles in the case of the impact of a spherical boulder.

To study the influence of particle shape, two sets of distributions of the parameters $a_i$ were calculated for the case of the impact of a boulder having a radius set at $R_b = R_m$ using soil samples composed of either spheres or clump particles. For both samples, the generation procedure consists of the deposition of particles under gravitational loading with a local friction angle set at 0° during the generation procedure. The generation procedure gave porosities of 0.204 and 0.171 for spheres and clump particles, respectively.

The difference between the distributions of the parameters $a_i$ obtained using spheres or clump particles cannot be considered negligible (Figure 7). Significant differences are observed for the terms associated with the rotational velocity of the impacting boulder ($a_{x\omega}$, $a_{y\omega}$, $a_{\omega x}$, $a_{\omega y}$, and $a_{\omega\omega}$). The use of clump particles induces differences in the shape of the soil surface, in the porosity of the soil, and in the contact force network. The surface of a soil composed with clump particles is composed of both quasi-planar and curved surfaces and is therefore very different to the surface of a soil composed with spherical particles. In addition, the rearrangement of clumps particles is easier which induces smaller porosity values and leads to very different contact force networks. Although the results do not allow separating the influence of each of these differences, they tend to emphasize the

predominant role of the differences in soil surface. Indeed, the shape of the surface of the soil plays an important role on the local incidence of the boulder. It therefore predominantly affects the parameters associated with the coupling between the rotational and the translational velocities.

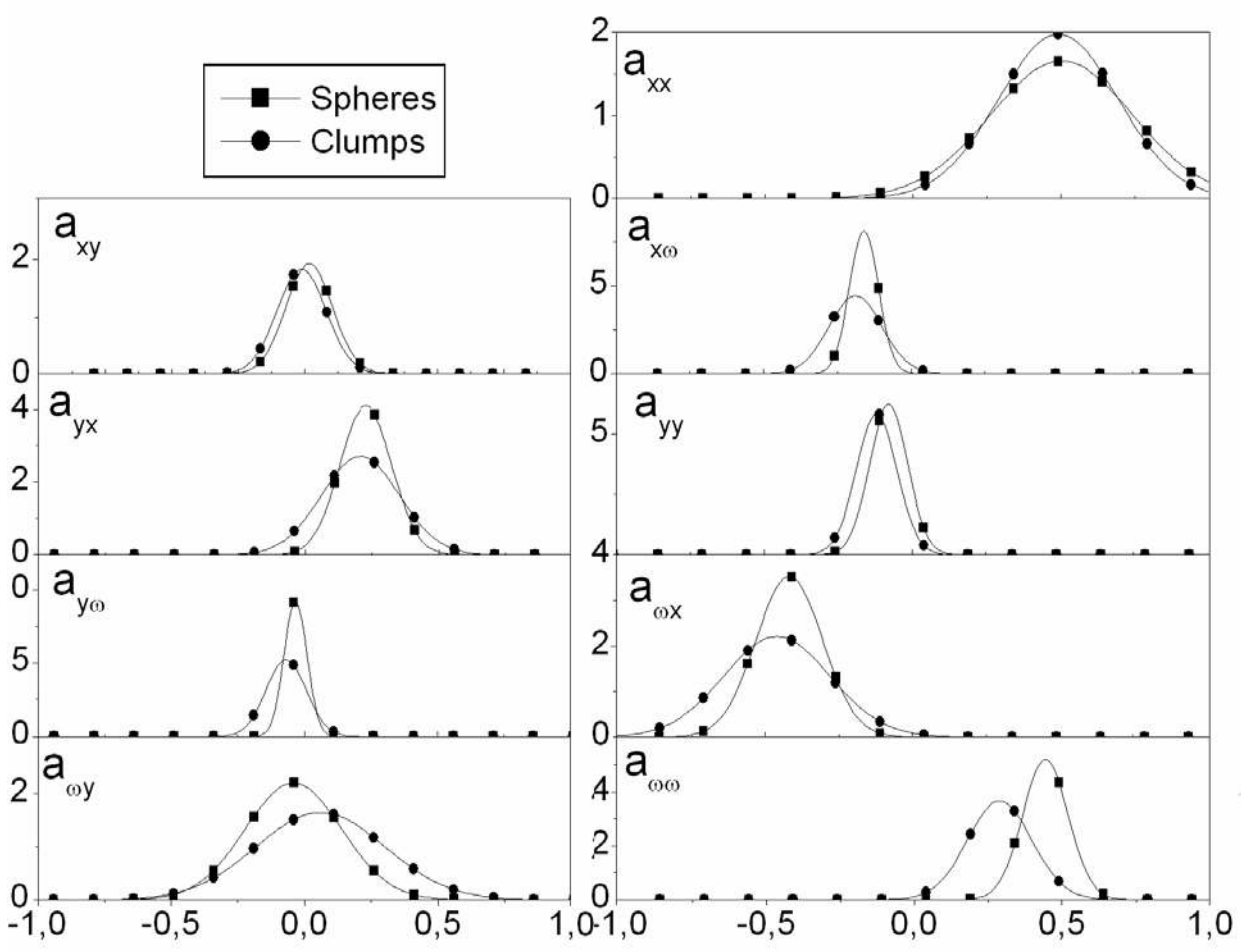


**Figure 7.** *Influence of particle shape on the distributions of the parameters* $a_i$

The physical processes involved during the impact vary greatly depending on the ratio of the falling boulder radius $R_b$ to the mean radius $R_m$ of the soil particles (Bourrier *et al.*, 2008). It is therefore advantageous to investigate whether the parameters of the stochastic bouncing model depend to a large extent on this ratio. The influence of the $R_b/R_m$ ratio is analyzed by calculating the parameters of the stochastic bouncing model using a soil sample composed of spherical particles with a porosity of 0.204. The $R_b/R_m$ ratio of the boulder radius to the mean radius of soil particles ranges within [0.5,5].

The mean values $m_i^a$ (Figure 8) and the standard deviations $s_i^a$ (Figure 9) of the parameters $a_i$ are highly dependent on the ratio $R_b/R_m$. The values of the parameters $m_i^a$ and $s_i^a$ differ greatly depending on whether the ratio $R_b/R_m$ is greater than 1. The physical phenomena leading to the impact process are indeed very different in these two domains (Bourrier *et al.*, 2008). It is also important to note that, for $R_b/R_m < 1$, the high values of the standard deviations $s_i^a$ stem from the high level of soil surface

roughness compared to the size of the impacting boulder. If the $R_b/R_m$ ratio is higher than 1, which corresponds to most practical cases, the variations in both parameters $m_i^a$ and $s_i^a$, depending on $R_b/R_m$, are smaller but they cannot be considered negligible. From a practical point of view, the variations observed clearly highlight that a single set of parameters $a_i$ is not sufficient to model the impact on a given soil type whatever the boulder size.

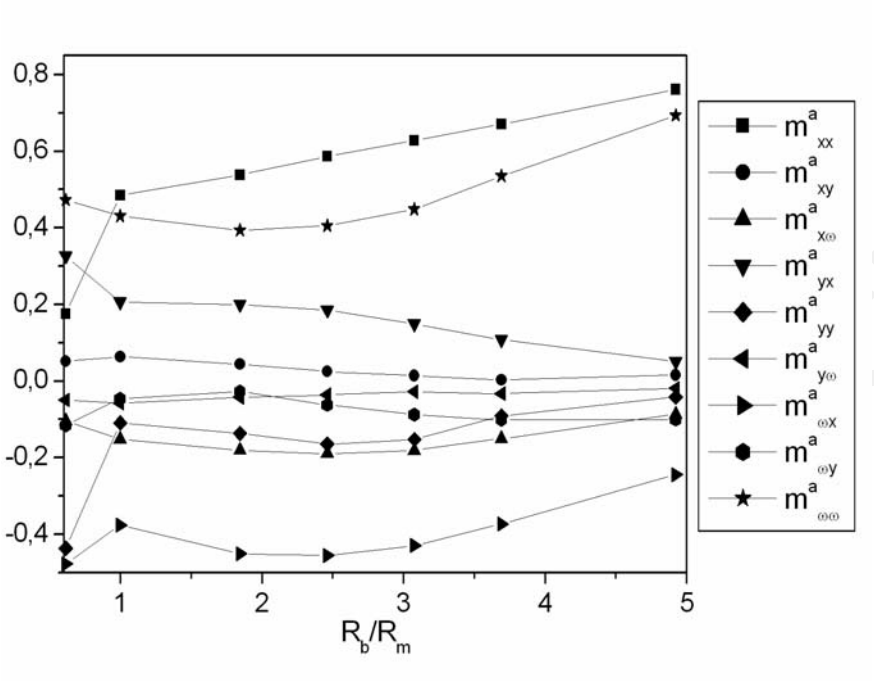


**Figure 8.** *Influence of the size of the boulder on the parameters $m_i^a$*

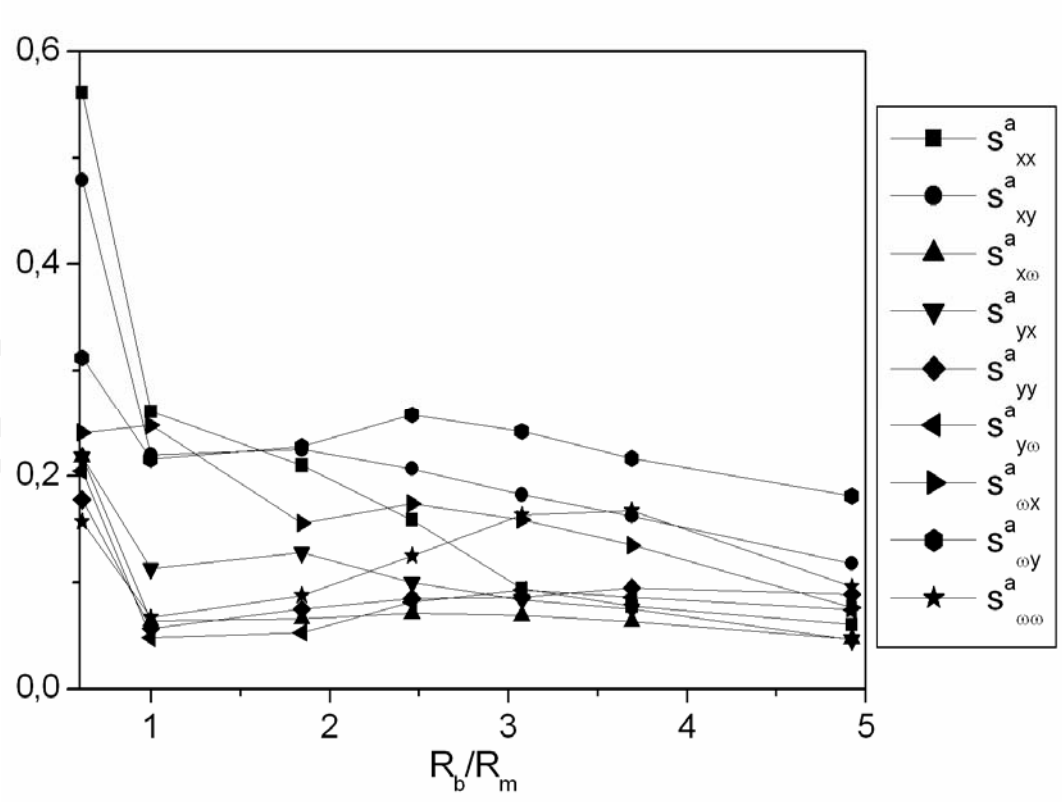


**Figure 9.** *Influence of the size of the boulder on the parameters $s_i^a$*

In conclusion, the influence of the shape of the soil particles and the boulder size was checked. Based on these results, the simplified stochastic bouncing model has to be given as a function of these two parameters. For practical purposes, given a soil (particle shape and size) and a boulder size, a set of given distribution of the parameters $a_i$ should be used. Interestingly, these parameters have a clear physical meaning and could be easily assessed from a field analysis. Moreover, it is worth noting that the soil properties (soil particle size and shape) can vary over the soil surface. These are local parameters. As a consequence, terms $a_i$ depend on the spatial coordinates of the point considered. In the next section, the ability of the simplified stochastic bouncing model for practical purposes is demonstrated.

## 4. Comparing the stochastic bouncing model with real-scale experimental results

The stochastic bouncing model proposed can precisely describe the variability of the reflected velocity for variable particle sizes and shapes and boulder sizes. Its application in the field of trajectory analysis can therefore be envisaged. The stochastic bouncing model is integrated into a 3D rockfall simulation model called Rockyfor (Dorren *et al*., 2004; Dorren *et al*., 2006). The rockfall simulation model developed was used to simulate real-scale rockfall experiments in order to evaluate the relevance of the stochastic bouncing model.

### 4.1. *Real-scale rockfall experiments*

The experimental site (Dorren et al. 2006) is located in the 'Forêt Communale de Vaujany' in France (lat. 45°12′, long. 6°3′). The study area covers an Alpine slope ranging from 1200 *m* to 1400 *m* above sea level with a mean gradient of 38°. The experimental site is part of a hill slope that is formed by a huge post-glacially developed talus cone mainly consisting of rock avalanche, snow avalanche, and rockfall deposits. The study site is about 100 *m* wide and 570 *m* long (distance between the starting point and the lower forest road, measured along the slope). It covers an avalanche path and is therefore denuded of trees.

During all the experiments the protocol was identical. Before each rockfall experiment, the volume of the boulder to be thrown was estimated by measuring the height, width, and depth along the three dominant boulder axes. A total of 100 boulders were released individually, one after the other. The mean volume of the boulders was 0.8 $m^3$ and the standard deviation 0.15 $m^3$.

A front shovel was used to throw the boulders down the slope, starting with a freefall of 5 *m*. At the end of each experiment, the stopping point of the boulders was captured. In addition, rockfall trajectories were filmed using five digital cameras, which were installed along the experimental site. Additional details on the experiments are given in Dorren *et al*. (2006).

The analysis of the digital films of the 100 rockfall trajectories provided the rebound heights, *i.e.*, the maximum vertical height between the center of the boulder and the slope surface, as well as the evolution of the velocity of the boulder for every $1/25^{th}$ second. Finally, the maximum value of the boulder velocity was recorded for each film.

### 4.2. *Trajectory simulations using the stochastic bouncing model*

As input data for the simulations of the real-scale experiments, the trajectory analysis software RockyFor first requires a Digital Elevation Model in which the topography and the rockfall source locations are fully defined. In general, a field survey defines the initial conditions for the calculation of the boulder's trajectory (rockfall source locations, boulder size, and the boulder's initial velocity vector), which were, in this case, equal to the initial experimental conditions.

For each rebound calculation, the reflected velocity vector was calculated from the incident velocity vector using the stochastic bouncing model. As the values of the parameters $a_i$ depend on the value of the ratio $R_b/R_m$ and on the shape of soil particles, a field survey should be conducted to determine the mean radius and the shape of soil particles in all points of the study site. In a first approximation, the spatial distribution of the soil particles' shape was not accounted for. Soil particles are assumed to be spherical at all points of the study site. However, a field survey was conducted to determine all the values of $R_m$ for all the spatial coordinates at the study site. The mean radius $R_m$ of the rocks covering the slope was determined in all points of the study site by identifying homogenous zones that are represented as polygons on a map. A value of the mean radius $R_m$ was estimated for each polygonal zone. Additionally, for each rockfall simulation, the spherical boulder radius $R_b$ was calculated using a sample value extracted from the distribution of the mass of the boulders used during the experiments.

A database was composed of several sets of the parameters $a_i$ for varying values of the $R_b/R_m$ ratio ranging from 1 to 5 which corresponds to classical values in the study site. To construct this database, DEM calculations were performed, which required evaluating soil properties that cannot be assessed in the field: the porosity and depth of the soil. Because of the different processes (snow avalanches, in particular) that occurred in the site, the soil is assumed to be dense at all points of the study site. The local friction angle was therefore set at 0° during the numerical soil sample generation, inducing a soil porosity of 0.204. In addition, the soil was assumed to be 4 *m* deep at all points of the study site.

As is usual in trajectory analysis, we chose to directly use the 2D stochastic bouncing model developed in a 3D context. In this context (Figure 10), the tangential and normal to soil surface components of the incident velocity vector allow definition of a plane called the incident plane. Similarly, the tangential and normal to soil surface components of the reflected velocity vector also allow

definition of a plane called the reflected plane. The angle $\delta^{re}$ between these two planes, which are perpendicular to soil surface, is called the deviation angle. In addition, the assumption is made that, before (or after) impact, the boulder's rotation axis is perpendicular to the incidence (or reflected) plane.

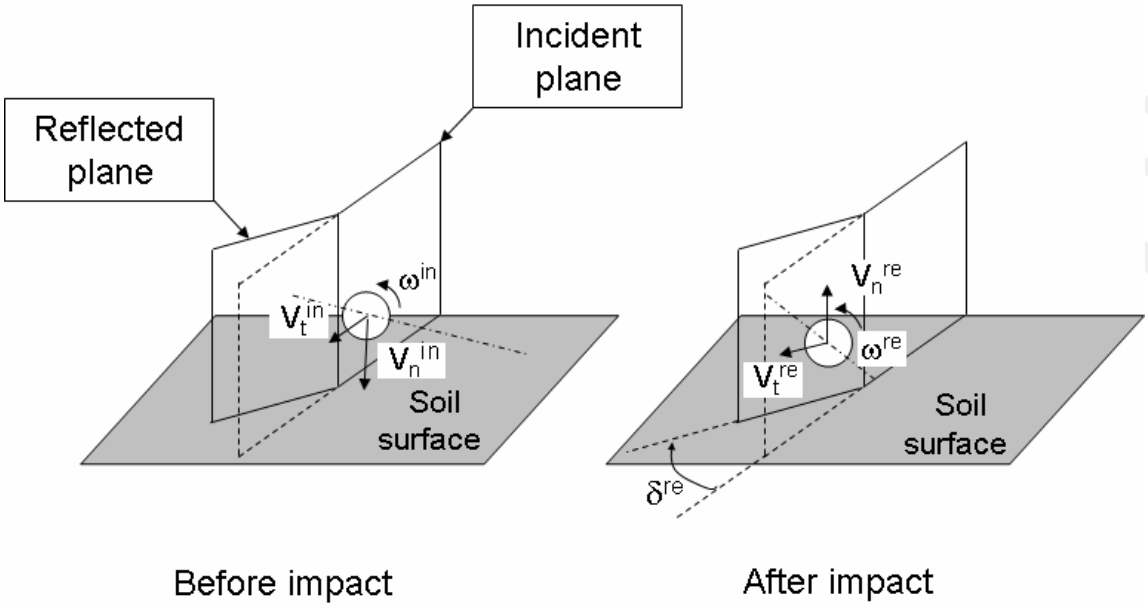


**Figure 10.** *Definition of the incident and reflected planes*

For each rebound of the boulder, the calculation of the reflected velocity vector from the incident velocity vector was performed in two stages.

The components of the reflected velocity vector in the reflected plane were first calculated from the components of the incident velocity vector in the incident plane using the stochastic bouncing model. For this purpose, the $R_b/R_m$ ratio was determined. This allows one to choose a set of parameters $a_i$ corresponding to the $R_b/R_m$ ratio calculated. The reflected velocity vector of the falling boulder was calculated using the set of parameters $a_i$ chosen from the stochastic bouncing model.

In the second stage, the deviation angle $\delta^{re}$ was calculated, leading to the complete definition of the reflected velocity vector. The deviation angle $\delta^{re}$ was determined by a random number that defines whether the rock is deviated, between 0 and 22.5º from its original direction toward the steepest slope direction, or 22.5–45º, or 45–55º. The first case has a probability of occurrence of 74%, the second case 24%, and the third case 4%. Additional details on the calculation of the deviation angle can be found in Dorren et al. (2004).

We carried out 10,000 rockfall simulations using the procedure described above. The simulated distributions of the maximum rebound heights $H^{max}$ and maximum translational kinetic energy $Ec^{max}$ were compared with the experimental distributions of those variables at one evaluation line (EL1), located 185 *m* from the starting point measured over the slope. In addition, the spatial patterns of the simulated trajectories

were compared with the spatial patterns observed during the real-scale rockfall experiments.

### 4.3. *Comparison between numerical results and real-scale experiments*

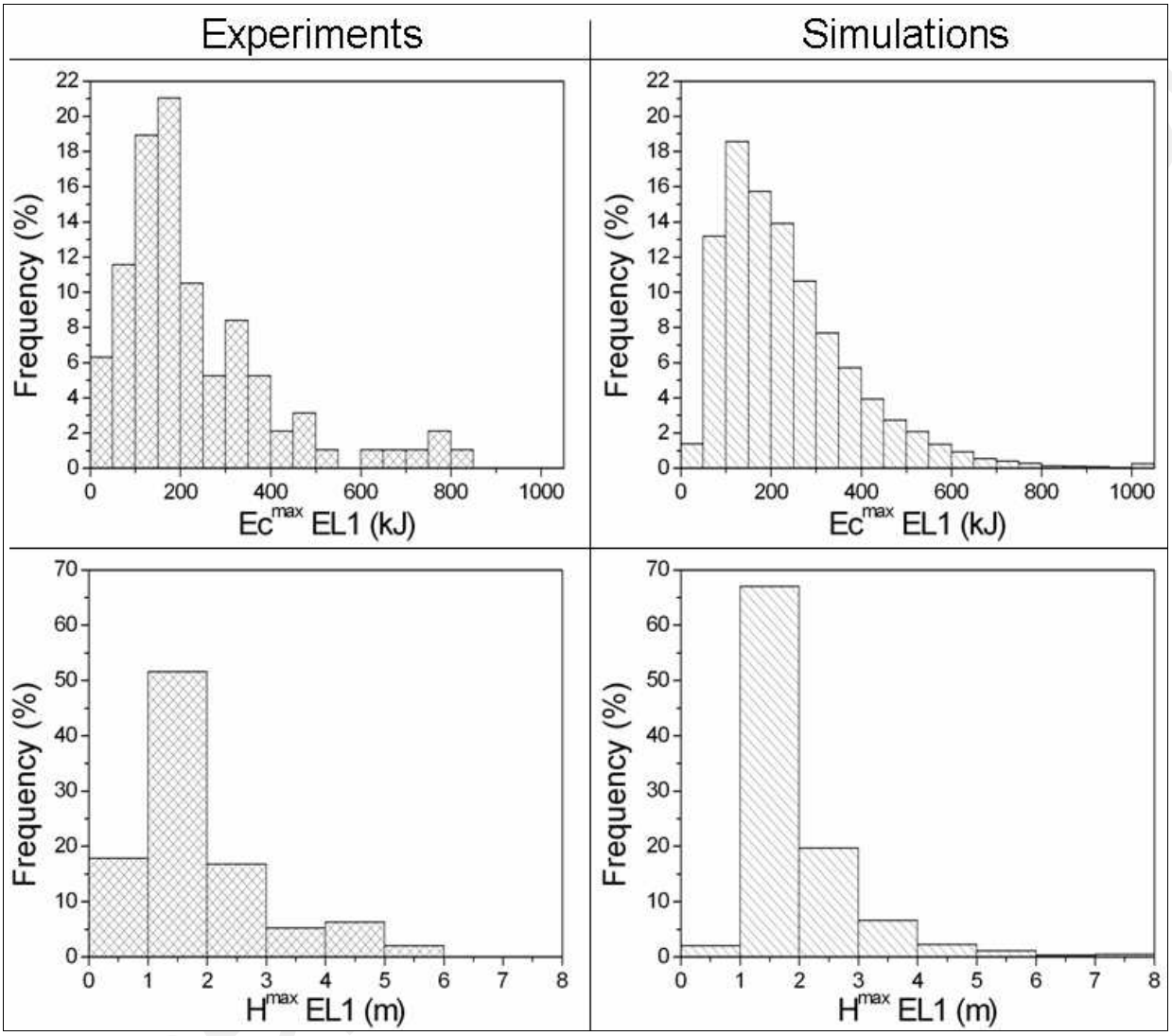


**Figure 11.** *Distribution of $H^{max}$ and $Ec^{max}$ for observed and simulated trajectories at EL1*

The comparisons between the experimental and simulated results at EL1 show that both the mean values and standard deviations are accurately reproduced by the simulations for boulder passing heights and translational kinetic energy (Table 2). The shapes of the distributions of the simulated quantities are very similar to those obtained from the experimental results, although the reduced number of experiments does not fully allow determination of the complete distribution (Figure 11). The simulated distributions can therefore be considered good predictions for the distributions of all quantities.

**Table 2.** *Mean values and standard deviations of $H^{max}$ and $Ec^{max}$ at EL1 obtained in the experiments and in the simulations after 10,000 simulation runs*

| | $H^{max}$ at EL1 (m) | | $Ec^{max}$ at EL1 (kJ) | |
|---|---|---|---|---|
| | Mean | Standard deviation | Mean | Standard deviation |
| Experiments | 1.4 | 1.1 | 205 | 169 |
| Simulations | 1.4 | 1.0 | 213 | 152 |

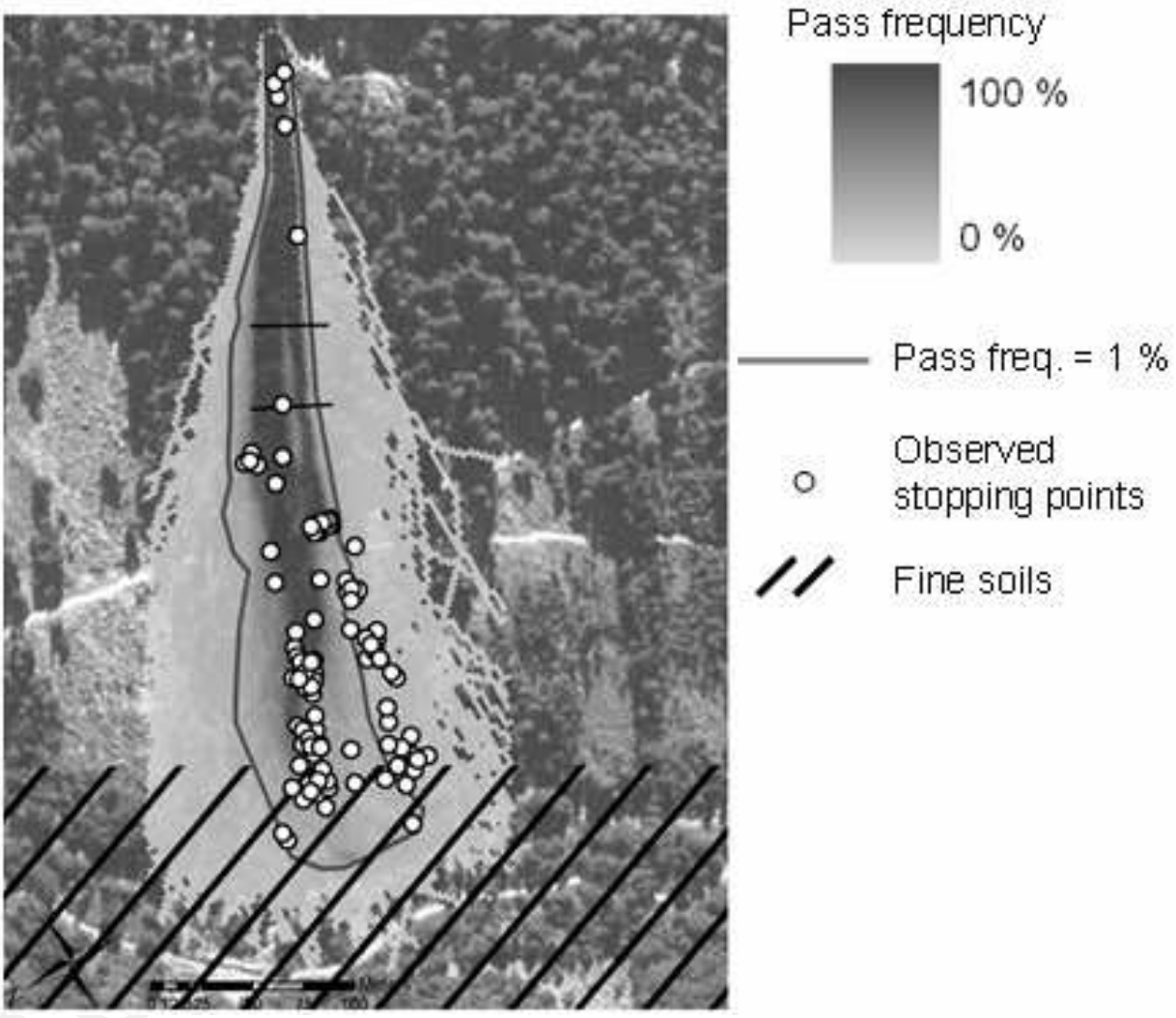


**Figure 12.** *Map of the simulated pass frequencies and observed stopping points (white dots with black outline)*

The 3D comparison between the simulated passing frequencies and the experimental stopping points of the falling rocks provides interesting information (Figure 12). First, the simulated runout zones in the simulations are larger than the area associated with the stopping points in the experiments. Indeed, the runout zone obtained in the simulations is associated with a probability of 1/10,000 that a

rockfall event occurs. On the other hand, as the real-scale experimental campaign consists of 100 rockfall experiments, the runout zone obtained in the experiments is associated with the 1% pass frequency limit. However, in the simulations, the limit for which the probability of a falling rock event is smaller than 1/100 (1% pass frequency limit) approximately corresponds to the experimentally observed stopping points. The rockfall simulation model therefore allows accurate simulation of the experimental runout zone associated with the 1% pass frequency.

The slight differences between simulated and experimental runout zones associated with the 1% pass frequency can be explained by the fact that the developed bouncing model is not adapted for surface material consisting of highly cohesive soils composed of fine particles, which is found in the valley bottom. The differences observed may also be due to an imperfect digital representation of the terrain in the Digital Elevation Model at the intersection of the avalanche path and the forest road. This local discrepancy in the Digital Elevation Model results from its spatial resolution.

However, the agreement between the model's predictions and the experimental results shows that integrating the stochastic approach presented in the field of trajectory analysis is relevant.

## 5. Conclusion

In this paper, a stochastic model for the bouncing of a boulder on a coarse soil was proposed. Since large data sets were necessary to perform the stochastic model determination, a numerical model of the impact using the DEM was first developed and validated compared with results from half-scale experiments. Based on this DEM model, an extensive numerical simulation campaign was carried out, providing a large set of results for varying local configurations of the soil and incident kinematic boulder parameters. The statistical analysis of the numerical results based on advanced statistical methods provides a definition of a stochastic bouncing model that quantifies most of the reflected velocity vector's variability.

The stochastic bouncing model developed can be considered an extension to classical models that simulate the coupling between the incident kinematic parameters. The global stochastic framework proposed also quantifies the sources of the variability in reflected velocity separately.

The detailed analysis of the model proves its relevance for modeling the variability of the reflected velocity vector for ratios of boulder size to soil particle mean size from 1 to 5. This analysis also highlights that the influence of soil particle shape cannot be ignored. Finally, the stochastic bouncing model proposed was used in the context of rockfall trajectory analysis to simulate real-scale rockfall experiments. The comparison between rockfall simulation and experimental results

proved the relevance of the stochastic bouncing model for performing rockfall trajectory simulations.

Thus, with the stochastic bouncing model, a coherent probabilistic starting point for carrying out prediction-oriented simulations of boulders impacting a coarse soil is proposed. In particular, probability distribution functions characterizing hazard levels on an endangered slope can be built, which offer objective probabilistic data for positioning and designing rockfall protective structures as well as hazard zoning.

Finally, the DEM model of the impact of a particle on a granular assembly presented in this paper is of great interest for investigating the physical mechanisms that govern boulder bouncing. In addition to the results presented in this paper, a detailed study of the mechanisms involved during the impact was conducted (Bourrier *et al*., 2008). The results obtained allowed thorough characterization of the energy exchanges between the impacting particle and the granular assembly, which resulted in defining three impact regimes depending on the size of the impacting particle and on the depth of the granular assembly. These results are interesting for several research fields such as aeolian sand transport or particle transport for industrial purposes.

## *6.* References


Agliardi F., Crosta G.B., "High resolution three-dimensional numerical modelling of rockfalls", *International Journal of Rock Mechanics and Mining Sciences*, vol. 40, 2003, p. 455-471.

Azzoni A., Rossi P.P., Drigo E., Giani G.P., Zaninetti A., "In situ observations of rockfalls analysis parameters", *Landslides*, Rotterdam, Balkema, Bell ed., 1991, p. 307-314.

Azzoni A., Barbera G.L., Zaninetti A., "Analysis and prediction of rockfalls using a mathematical model", *International Journal of Rock Mechanics and Mining Sciences*, vol. 32, 1995, p. 709-724.

Bayes T., "Essay towards solving a problem in the doctrine of chances", *Philosophical Transactions of the Royal Society of London*, vol. 53, vol. 54, 1763, p. 370-418, p. 296-325.

Berger J.O., *Statistical Decision Theory and Bayesian Analysis. 2nd edition*, Springer-Verlag, 1985.

Bertrand D., Nicot F., Gotteland P., Lambert S., Derache F., "Modelling a geo-composite cell using discrete analysis", *Computer & Geotechnics*, vol. 32, n° 8, 2006, p. 564-577.

Bourrier F., Nicot F., Darve F., "Rockfall modelling: Numerical simulation of the impact of a particle on a coarse granular medium", *Proc. 10th Int. Congr. on NUmerical MOdel in Geomechanics*, Pietruszczak and Pande eds., Taylor & Francis, 2007, p. 699-705.

Bourrier F., Nicot F., Darve F., "Physical processes within a 2D granular layer during an impact", *Granular Matter*, vol. 10, n° 6, 2008, p. 415-437.

Box G.E.P., Tiao G.C., *Bayesian Inference in Statistical Analysis*, Addison-Wesley, 1973.

Bozzolo D., Pamini R., "Simulation of rockfalls down a valley side", *Acta Mechanica*, vol. 63, 1986, p. 113-130.

Brooks S.P., "Markov Chain Monte Carlo Method and its application", *The Statistician*, vol. 47 n° 1, 1998, p. 69-100.

Cundall P.A., Strack O.D.L., "A discrete numerical model for granular assemblies", *Geotechnique*, vol. 29, 1979, p. 47-65.

Cundall P.A., "Computer simulations of dense spheres assemblies", *Micromechanics of Granular Materials*, Amsterdam, Elsevier Science Publisher B.V., M. Satake & J.T. Jenkins eds., 1988, p. 113-123.

Deluzarche R., Cambou B., "Discrete numerical modelling of rockfill dams", *Int. J. Numer. Anal. Meth. Geomech.*, vol. 30, 2006, p. 1075-1096.

Dimnet E., Fremond M., "Instantaneous collisions of solids", *European Congress on Computational Methods in Applied Sciences and Engineering*, 2000, p. 11-17.

Dorren L.K.A., Maier B., Putters U.S., Seijmonsbergen A.C., "Combining field and modelling techniques to assess rockfall dynamics on a protection forest hillslope in the European Alps", *Geomorphology*, vol. 57 n° 3, 2004, p. 151-167.

Dorren L.K.A., Berger F., Putters U.S., "Real-size experiments and 3-D simulation of rockfall on forested and non-forested slopes", *Natural Hazards and Earth System Sciences*, vol. 6, 2006, p. 145-153.

Evans S.G., Hungr O., "The assessment of rockfall hazard at the base of talus slopes", *Canadian Geotechnical Journal*, vol. 30, 1993, p. 620-636.

Falcetta J.L., "Un nouveau modèle de calcul de trajectoires de blocs rocheux", *Revue française de géotechnique*, vol. 30, 1985, p. 11-17.

Fisher R.A., "Probability, likelihood and quantity of information in the logic of uncertain inference", *Proc. Roy. Soc. A.*, vol. 146, 1934, p. 1-8.

Frattini P., Crosta G.B., Carrara A., Agliardi F., "Assessment of rockfall susceptibility by integrating statistical and physically-based approaches", *Geomorphology*, vol. 94 n° 3-4, 2008, p. 419-437.

Gilks W.R., Richardson S., Spiegelhalter D.J., *Markov Chain Monte Carlo in Practice*, New-York, Chapman & Hall, 2001.

Goodman R.E., *Introduction to rocks mechanics*, Boston, PWS Publishing Company, 1980.

Guzzetti F., Crosta G., Detti R., Agliardi F., "STONE: a computer program for the three dimensional simulation of rock-falls", *Computer & Geosciences*, vol. 28, 2002, p. 1079-1093.

Itasca Consulting Group., *PFC2D User's manual*, Minneapolis, Itasca, 1999.

Jaboyedoff M., Dudt J.P., Labiouse V., "An attempt to refine rockfall zoning based on kinetic energy, frequency and fragmentation degree", *Natural Hazards and Earth System Sciences*, vol. 5, 2005, p. 621-632.

Kirkby M.J., Statham I., "Surface movement and scree formation", *Journal of geology*, vol. 83, 1975, p. 349-362.

Kobayashi Y., Harp E.L., Kagawa T., "Simulation of rockfalls triggered by earthquakes", *Rocks Mechanics and Rock Engineering*, vol. 23, 1990, p. 1-20.

Koo C.Y., Chern J.C., "Modification of the DDA method for rigid blocks problems", *International Journal of Rock Mechanics and Mining Sciences*, vol. 35 n° 6, 1998, p. 683-693.

Laouafa S., Nicot F., "Modélisation numérique de l'impact d'un bloc rocheux sur un sol composé d'éboulis", *Revue française de géotechnique*, vol. 109, 2003, p. 87-97.

Mindlin R.D., Deresiewicz H., "Elastic spheres in contact under varying oblique forces", *Journal of Applied Mechanics*, vol. 20, 1953, p. 327-344.

Neyman J., Pearson E.S., "On the testing of statistical hypothesis in relation to probability a priori", *Proc. Cambridge Phil. Soc.*, vol. 29, 1933, p. 492-510.

Nicot F., Gotteland P., Bertrand D., Lambert S., "Multiscale approach to geo-composite cellular structures subjected to rock impacts", *Int. J. Numer. Anal. Meth. Geomech.*, vol. 31, 2007, p. 1477-1515.

Oger L., Ammi M., Valance A., Beladjine D., "Discrete Element Method to study the collision of one rapid sphere on 2D and 3D packings", *Eur. Phys. J. E*, vol. 17, 2005, p. 467-476.

Paronuzzi P., "Probabilistic approach for design optimization of rockfall protective barriers", *Quarterly Journal of Engineering Geology*, vol. 22, 1989, p. 175-183.

Pfeiffer T.J., Bowen T.D., "Computer simulations of rockfalls", *Bulletin of the Association of Engineering Geologists*, vol. 26, 1989, p. 135-146.

Spiegelhalter D.J., Thomas A., Best N., *WinBUGS Version 1.3 User Manual*, MRC Biostatistics Unit, 2000.